Mohanty, D.; Gabrisch, H.:

Microstructural investigation of LixNi1/3Mn1/3Co1/3O2 (x ≤ 1) and its aged products via magnetic and diffraction study

In: Journal of Power Sources (2012) Elsevier

DOI: 10.1016/j.jpowsour.2012.08.005

Microstructural investigation of $Li_xNi_{1/3}Mn_{1/3}Co_{1/3}O_2$ ($x \leq 1$) and its aged products via magnetic and diffraction study

D. Mohanty[1,*] and H. Gabrisch[2]

[1]Advanced Materials Research Institute, University of New Orleans,

New Orleans, LA 70148, USA

[2] Helmholtz-Zentrum Geesthacht, Institute of Materials Research, Department of Metal Physics,

Max-Planck-Str.1, 21502 Geesthacht, Germany

Abstract

The thermal stability of the layered oxide $LiNi_{1/3}Mn_{1/3}Co_{1/3}O_2$ and its delithiated product is studied by a combination of x-ray and electron diffraction, TEM imaging and magnetic measurements. Diffraction shows that a small fraction of the layered material converts to spinel phase following delithiation. More spinel phase is observed after thermal annealing. The morphology of the particle changes upon thermal annealing of delithiated materials. The selected area electron diffraction and the magnetic measurement results confirm the presence of Ni^{+2}/Li^{+} disorder in the delithiated material, which increases upon thermal ageing. The oxidation states of the transition metal ions were determined from magnetic data. It is shown that the charge balance due to the removal of Li^{+} is maintained through oxidation of Ni^{+2} and that the oxidation states remain stable during subsequent annealing. No anti-ferromagnetic ordering or crystallographic in plane ordering of transition metal ions is observed. These results clearly describe the thermal degradation of $Li_xNi_{1/3}Mn_{1/3}Co_{1/3}O_2$ ($x \leq 1$) occur through the significant microstructural changes.

Key words: Magnetic ordering, electron diffraction, thermal ageing, spinel

*Corresponding author: Debasish Mohanty, email: mohantyd@ornl.gov
Address: Materials Science and Technology Division, Oak Ridge National Laboratory,
Oak Ridge, Tennessee, 37931-6083, USA. Tel: +1 865 576 0813

1. Introduction

Rechargeable lithium-ion batteries (LIBs) are popular power sources for consumer electronic devices such as cellular telephones, digital cameras, camcorders, and laptop computers. [1-2] Due to their high energy density and high capacity, LIBs are also being considered as energy storage devices for hybrid electric vehicles (HEVs), Electric vehicles (EVs), biomedicine, and space. Despite this success, there is a need to improve safety, energy density and life span of LIBs while reducing costs. Layered oxide materials of the composition $LiMO_2$ (M=Co, Mn, Ni) have attracted much attention as potential candidates for cathodes in LIBs.[3] Especially the ternary transition metal oxide $LiNi_{1/3}Mn_{1/3}Co_{1/3}O_2$ is considered one of the most promising cathodes in high power rechargeable Li-ion batteries for application in hybrid electric vehicles (HEVs) due to its good thermal stability and high reversible capacity [4-7]. $LiNi_{1/3}Mn_{1/3}Co_{1/3}O_2$ adopts to the $NaFeO_2$ structure described by the $R\bar{3}m$ space group (O3 phase) which is formed by sheets of edge sharing MO_6 octahedra [M= Ni, Mn, Co] separated by layers of lithium ions in octahedral interstitial sites. The different species of transition metal ions play significant roles regarding the stability and electrochemical activity of this compound. It has been shown that Nickel (Ni^{+2}) is the electrochemical active species, manganese (Mn^{+4}) provides structural stability and cobalt (Co^{+3}) supports ordering of lithium and nickel ions onto their respective lattice sites [8]. Due to the similar ionic radii of Ni^{+2} (0.67Å) and Li^{+} (0.76Å) there is always a chance that these two ions are exchanged on their crystallographic sites [9-10] which introduces local disorder that may impair the electrochemical performance[11]. Another problem is that early during charge of the battery Ni^{+2} ions in the lithium layers are oxidized to Ni^{+3} ions before lithium is removed. The Ni^{+3} ions distort the lithium layers, thereby impeding the lithium diffusion [10,12]. The Li^{+}/Ni^{+2} interchange also initiates the possibility that cations in the transition metal layers take on various ordering schemes which may affect the electrochemical activity[13]. Experimental evidence for in-plane ordering has been observed first by Yabuuchi et. al who studied the pristine material by electron

diffraction. The authors reported the formation of a $\sqrt{3}$ x $\sqrt{3}$ R30^{o} in plane unit cell that is identified by superlattice reflections [7]. In our own previous work on commercially produced $LiNi_{1/3}Mn_{1/3}Co_{1/3}O_2$ we found that the pristine material was comprised of a mixture of particles having either random cation distribution (O3 structure), long-range $\sqrt{3}$ x $\sqrt{3}$ R30^{o} in plane ordering or a cubic spinel structure [13, 14]. Using electron diffraction we monitored the change in relative amounts of phases after ageing, electrochemical cycling or charge to a high voltage of 5.2V. We also observed a structural degradation after repeated charge discharge cycling where thin layers of the $LiNi_{1/3}Mn_{1/3}Co_{1/3}O_2$ powder particles were split parallel to the (0001) basal plane ('mille feuille' morphology) [14].

Single crystal diffraction studies provide important information on ordering schemes within individual particles of a compound but not on the nature of the species involved or their oxidation state. Information on oxidation states of transition metal ions[15], cation ordering,[16-17] stoichiometry of lithium ions[18] can be deduced from the magnetic data of these oxides . For example, magnetic measurements of $LiCoO_2$ were used to characterize changes in the oxidation state of cobalt ions upon lithium extraction [19-21]. In our own previous studies on Li_xCoO_2 we used a combination of this "magnetic tool" and diffraction techniques to identify Co_3O_4 and $LiCo_2O_4$ as products of thermal decomposition .[22] Subsequently we extended the approach of combined electron diffraction and magnetic measurements to the binary system $LiNi_{1-x}Mn_xO_2$ [18] and finally to the ternary $LiNi_{1/3}Mn_{1/3}Co_{1/3}O_2$ compound. Although the magnetic properties of the ternary $LiNi_{1/3}Mn_{1/3}Co_{1/3}O_2$ material has been described in several studies [15,23,16], to our knowledge, no reports can be found where the magnetic properties are correlated to electron diffraction studies in an attempt to understand the cation ordering in this material. Here we present studies on the magnetic behavior of $LiNi_{1/3}Mn_{1/3}Co_{1/3}O_2$ and its delithiated product before and after ageing accompanied by selected area electron diffraction studies. The magnetic response of mixed

transition material is strongly dependent on the cation ordering in the transition metal layers and on the presence of small amounts of Ni^{+2} in the Li-layer. Both generate ferromagnetic (180° interlayer Ni^{+2} - O - Mn^{+4}) and/or antiferromagnetic (180° interlayer Ni^{+2} - O - Ni^{+2}) ordering of some degree and can be detected by magnetic measurements. At the same time Ni^{+2}/Li^{+} interchange can be detected by single crystal electron diffraction data where either forbidden {1-100} reflections appear as a direct consequence of the presence of a Ni^{+2} ion in the Li-layer or by superlattice reflections appears due to long range order in the transition metal layer[24] .

2. Experimental

$LiNi_{1/3}Mn_{1/3}Co_{1/3}O_2$ was prepared by the hydroxide co-precipitation method following the modified procedure reported by Lue et al.[25]. Briefly, stoichiometric amounts of $NiSO_4 \cdot 6H_2O$, $CoSO_4 \cdot 7H_2O$ and $MnSO_4 \cdot H_2O$ with a Ni:Co:Mn ratio of 1:1:1 were dissolved separately in distilled water to prepare $2molL^{-1}$ solutions. These solutions were mixed together and then stirred continuously for 1h at 50 ^{O}C under argon atmosphere. 50 mL of aqueous NaOH and NH_4OH solution were added to obtain precipitates maintaining pH of 10-11. The solution was stirred in argon atmosphere for 24 h at 50 °C. Then the precipitate was filtered, washed with water and kept at 50^{o}C overnight to dry. The precursor was then mixed with a stoichiometric amount of $LiOH \cdot H_2O$ and thoroughly ground by mortar and pestil. The powder was pressed into pellets, heated at 450^{o}C for 5h followed by heating at 650^{o}C for 9h. The disintegrated pellets were pressed again, calcinated at 850^{o}C for 18hrs and ground to obtain black $LiNi_{1/3}Mn_{1/3}Co_{1/3}O_2$ powder. Chemical delithiation was performed under argon atmosphere at room temperature using a solution of NO_2BF_4 in acetonitrile in a concentration ratio of TM: oxidant equal to 1 : 1.1. The reaction was carried out by drop wise addition of NO_2BF_4 over 90 minutes followed by additional stirring for 90 minutes to produce $Li_{1-x}Mn_{1/3}Co_{1/3}O_2$. Subsequently portions of the delithiated powder were annealed in air at 75ºC for 30 days and for 45 days (hereafter abbreviated as 75C 30

d and 75C 45 d) respectively. Quantitative analysis of the Co, Mn, Ni and Li content was carried out through Inductive Coupled Plasma Mass Spectrometry (ICP-MS) on the starting material and its delithiated compounds. X-ray diffraction spectra (XRD) were collected with an X'pert PRO diffractometer (PANalytical) operated at 40kV voltage and 40mA current using Cu-Kα radiation. Silicon powder was mixed into the powders as diffraction standard. Phase determination was carried out by comparison between experimental and simulated powder diffraction spectra. The simulations were obtained with the software "Powder cell" and using unit cells published in literature [26]. Magnetic measurements were performed under field cooling (FC) and zero field cooling (ZFC) using a superconducting quantum interface (SQUID) magnetometer (MPMS-XL-7: Quantum Design) in the temperature range between 5K-300K under a magnetic field H=10kOe. The plots of magnetic moment and magnetic field (M-H) curves were obtained the same instrument at T=5K. Transmission electron micrographs and selected area electron diffraction patterns were obtained using the JEOL 2010 Transmission Electron Microscope at the University of New Orleans operated at 200 kV. Experimental diffraction patterns were compared to patterns simulated with the software Desktop Microscopist.

3. Results and discussion

3.1. Pristine and delithiated material ($Li_xCo_{1/3}Mn_{1/3}Ni_{1/3}O_2$, x=1, 0.80)

3.1.1 X-ray diffraction and magnetic behavior before and after delithiation

Fig. 1 a, b represent x-ray powder diffraction patterns of the starting material and its delithiated products. In the starting material all peaks can be indexed according to the $R\bar{3}m$ space group (space group no. 166). The c and a lattice parameters are 14.135 Å and 2.84 Å respectively with c/a ratio of 4.97 which is in agreement with values reported in literature[25]. The clear splitting

of (006)/ (102) and (108)/ (110) doublets in the starting material illustrates the presence of a layered structure. The ratio of I_{003} /I_{104} is higher than the value of 1.2 which confirms that the material has crystallized in a layered structure. Similarly a low R-factor (R= $(I_{102}+I_{006})/I_{101}$) is considered a good estimate on the separation of TM ions and Li ions onto their respective planes in a layered structure [27]. Here the *R*- factor for the starting material has a value of 0.391 which is significantly lower than values reported in literature[25]. After chemical delithiation the (003) peak shifts to lower 2θ values corresponding to an increased c lattice parameter (14.384 Å) compared to the starting material (see the inset of figure 1). The spacing between the peaks in the (006)/(012) and (108)/(110) doublets increases after deintercalation of lithium ions. This is caused by the electrostatic repulsion among the MO_2 (M= Co, Mn, Ni) slabs along c direction of the unit cell as lithium is extracted from the parent layered structure. After delithiation, decrease in a-lattice parameter (See table 1) was observed. This is attributed to the decrease in average metal-metal distance due to formation of ions having smaller effective ionic radii. In $Li_xCo_{1/3}Mn_{1/3}Ni_{1/3}O_2$, Ni^{+2} is electrochemically active ions and the charge compensation during lithium extraction must have been accompanied by the oxidation of Ni^{+2} (0.69 Å) to Ni^{+3} (0.56 Å)/ Ni^{+4} (0.48 Å). Overall, no phase change was observed by XRD after lithium extraction.

The temperature dependence of the magnetic susceptibility of the starting material and its delithiated product measured under field cooling (FC) and zero field cooling (ZFC) is shown in figure 2. Above 100K both compounds show paramagnetic behavior obeying the Curie Weiss law. Below 100 K an increase in magnetic susceptibility is observed that is more pronounced for the starting material than for the delithiated product. This means that less magnetic moment is present in the compound after delithiation. The oxidation state of cobalt, nickel and manganese ions in the two compounds were determined from a comparison of the experimentally measured effective magnetic moments to calculated theoretical magnetic moments. The measured effective magnetic moments were obtained from the plot of inverse molar susceptibility vs. temperature in

the temperature region 100K-300K using the equation $\chi_m = C_m/(T-\theta)$. Here χ_m is the molar magnetic susceptibility, C_m is the Curie constant, and θ is the Weiss temperature. The experimentally obtained effective magnetic moments are 2.69 ± 0.01 μ_B for the starting material and 2.33 ± 0.1 μ_B for the delithiated material. The theoretical effective moments were calculated using the chemical composition measured by ICP and considering the following magnetic states: Mn^{+4} (HS/LS), Co^{+3} (LS), Ni^{+2} (HS/LS), Ni^{+3} (HS/LS) and Ni^{+4} (HS/LS). The Co^{+4} (HS/LS) was not considered for calculating theoretical effective magnetic moment in delithiated material. Because, in literature[28] it has been reported that the oxidation of Co^{+3} to Co^{+4} takes place at higher lithium deficiency (high voltage) and therefore intercalation mechanism in $LiCo_{0.33}Mn_{0.33}Ni_{0.33}O_2$ was attributed to the Ni^{+2}/Ni^{+4} redox reaction.[28] The composition of the starting material and the delithiated material were determined to be $LiCo_{0.33}Mn_{0.33}Ni_{0.33}O_2$ and $Li_{0.80}Co_{0.33}Mn_{0.34}Ni_{0.34}O_2$ respectively with an error margin of ±0.02 mol. The experimental effective magnetic moment of the starting material (2.69 μ_B) is best explained by a combination of 0.33mols of Ni^{+2} (HS; S= 1), 0.33mols of Mn^{+4} (HS; S=3/2) and 0.33moles of Co^{+3} (HS; S=0) which corresponds to a theoretical effective magnetic moment of 2.77 μ_B. During delithiation 20% of the lithium ions are extracted from the lattice, which may be compensated for by the oxidation of 0.10 mol Ni^{+2} to Ni^{+4} or by oxidizing 0.20 mol of Ni^{+2} to Ni^{+3}. The experimental effective magnetic moment after delithiation (2.33 μ_B) is best described by the composition $Li_{0.80}Co_{0.33}{}^{+3(LS)}Mn_{0.34}{}^{+4(HS/LS)}Ni_{0.23}{}^{+2(HS/LS)}Ni_{0.10}{}^{+4(LS)}O_2$ corresponding to a theoretical effective magnetic moment of 1.76μ_B. For comparison the theoretical effective magnetic moment resulting from the oxidation of Ni^{2+} to Ni^{3+} would be 1.40μ_B (Ni^{+3}, LS) and 1.55μ_B (Ni^{+3}, HS). This suggests that the delithiation process primarily involves the oxidation of Ni^{+2} (S=1) to Ni^{+4} (S=0) ions. It is evident that, the experimental effective magnetic moment for the delithiated sample is higher than the theoretical effective magnetic moment (2.33 μ_B compared to 1.76μ_B) The discrepancy of 0.57μ_B between experiment and model in the delithiated material could be

explained by presence of 1.) a small amount of magnetic Ni^{+3} (LS or HS, S=1/2 or 3/2) or 2.) Ni^{+4} in high spin state (HS, S=2) in the place of Ni^{+4} (LS, S=0). In detail 0.013 mole of Ni^{+4} (HS) or 0.022 mole of Ni^{+3} (HS) or 0.11 mole of Ni^{+3} (LS) ions could compensate the difference between theoretical and experimental value of the effective magnetic moment. The presence of Ni^{+3} in the transition metal layer can be excluded based on the fact that the presence of Ni^{+3} and Mn^{+4} in the transition metal layer can create the magnetic frustrated lattice with the Ni^{+2} in the lithium layer[17](see the discussion in later sections). Therefore, it can be concluded that the presence of Ni^{+4} (HS) causes the high experimental magnetic moment which was observed in the delithiated material.

To investigate the Ni^{+2} /Li^{+} exchange in the starting and delithiated material, a plot of magnetic field (H) vs. magnetic moment (M) at *T*=5K is shown in figure 3. Both materials show similar behavior at that temperature without hysteresis behavior. However, the curve for the lithium deficient material has a significantly steeper slope than the curve of the starting material. This suggests that the lithium deficient material deviates from paramagnetic character at *T*=5K. The higher slope of the M(H) curve in the lithium deficient material indicates the presence of some small degree of ferromagnetic interaction that could be due to the presence of Ni^{+2} in the lithium layer. Strong ferromagnetic ordering would be evident if a hysteresis loop was observed in the M(H) curve – which is not the case here. Therefore, in the present case it is reasonable to assume that the amount of Ni^{+2}-Li^{+} interchange is not sufficient to create a strong ferromagnetic ordering despite of the slope change of M-H curve. This conclusion is supported by the single crystal electron diffraction data where after delithiation only a few particles having faint forbidden {1-100} reflections were found suggesting some degree of Li^{+}/Ni^{2+} interchange (see the discussion below).

A comparison of the magnetic response of the ternary $Li_xNi_{1/3}Mn_{1/3}Co_{1/3}O_2$ ($x\leq1$) to the "mono" atomic system Li_xCoO_2 ($x\leq1$) and to the binary $Li_yNi_{1-x}Mn_xO_2$ ($y\leq1$; $x=0.3,0.5,0.7$) illustrates the behavior of the TM species [17,22]. In case of Li_xCoO_2 the starting material is

paramagnetic over the temperature region *T*=5K-300K [22,29]. After continuous lithium extraction an increase in magnetic susceptibility (and increase in effective magnetic moment) was observed because the lithium extraction process involves the oxidation of Co^{+3}(LS, S=0) to Co^{+4} (HS; S=5/2 and/or LS; S=1/2). As long as the layered character is maintained no magnetic exchange interaction is observed in the "mono" atomic Li_xCoO_2 system. In the binary system $Li_yNi_{1-x}Mn_xO_2$ ($y\leq1$; x=0.3, 0.5, 0.7) the interaction between two magnetic ions (Mn and Ni) is possible as described by Goodenough's rule[30]. The nature and strength of the interaction depends on the spin state and the relative alignment of the magnetic cations through the oxygen anion (90 degree or 180 degree). Strong ferromagnetic coupling due to 180^o ferromagnetic interaction between Ni^{+2} (in lithium layer)-O-Mn^{+4} (in TM layer) is indeed observed at a Mn^{4+} to Ni^{2+} ratio of 1:1 in $LiNi_{0.5}Mn_{0.5}O_2$ [17]. This ferromagnetic coupling was less pronounced in Ni rich composition and absent in Mn rich compositions where instead a paramagnetic behavior was observed. Li-extraction changed the oxidation state of Ni^{+2} (LS/HS; S=1) to Ni^{+3} (LS ;S=1/2) and/or Ni^{+4} (LS;S=0) and the effective magnetic moments are lower compared to those of the starting material. The ternary system, $Li_xNi_{1/3}Mn_{1/3}Co_{1/3}O_2$ ($x\leq1$), is comparable to the binary one as far as only Mn^{+4} and Ni^{+2} ions are magnetically active in the fully lithiated state and charge compensation during Li-extraction is realized by the oxidation of Ni^{2+}. On the other hand the compound is paramagnetic despite having a Ni:Mn ratio of 1:1 indicating that no Ni^{+2}/Li^+ exchange occurs in the fully lithiated state, possibly because of the stabilizing role of Co ions. The magnetic susceptibility of the delithiated specimen is lower than that of the starting material since the lithium extraction changes the oxidation states of of Ni^{+2} (LS/HS; S=1) to Ni^{+3} (LS ;S=1/2) and/or Ni^{+4} (LS;S=0).

3.1.2 Microstructure before and after delithiation

The crystal structure of individual powder particles of the starting material and its delithiated product was monitored by single crystal electron diffraction. The observed diffraction patterns are classified into the categories : O3 phase (random cation distribution on 3a sites), cubic spinel phase (SG 227, TM ions on octahedral 16d, Li 16c) , forbidden {1-100} reflections (Ni^{2+} in Li layer), and in-plane ordering (long range order of cations in TM layer enabled by presence of Li ions in TM layer)[24]. A summary of the results is given in table 3. In the starting material 20 out of 22 particles (or 90%) were indexed as O3 phase and the remaining 2 particles or 10% were indexed as spinel phase. This suggests that the transition metal ions are randomly distributed over 3a lattice sites in the starting material and that no Li^{+}/Ni^{+2} interchange or long range order in the TM layer occur. This clearly establishes the fact that the synthesis process was successful to produce homogeneous $LiNi_{1/3}Mn_{1/3}Co_{1/3}O_2$ without in-plane ordering. For comparison about 10% of particles showed in plane ordering in our previous investigation [24]. The appearance of small number of particles showing spinel phase is not fully understood. However, it is assumed that, during synthesis process a little number of particles with spinel phase has been formed. An illustration of a particle having a typical O3-type diffraction pattern is given in figure 4 b. The morphology of the pristine particles before chemical delithiation was smooth across the edge of the particle surfaces (figure 4 a).

After chemical delithiation some powder particles showed corroded edges resulting from the etching process (see the figure 5 a). Analysis of the diffraction patterns of 20 particles of the delithiated powder showed that the amount of spinel phase had increased at the expense of the amount of O3 phase, see table 3. Additionally particles with weak intensities at the position of forbidden {10-10} reflections were observed. Out of 20 particles 12 (or 60%) were indexed as O3 phase, 4 (or 20 %) showed spinel reflections and 20% showed weak forbidden {10-10}

reflections. An example for the appearance of faint forbidden reflections is given in figure 5 b. This observation differs from the observations in the chemically delithiated Li_xCoO_2 where the removal of small amounts of lithium results in the appearance of strong forbidden {1-100} reflections in [0001] zone axis direction which clearly suggests the improved structural stability of the mixed TM compounds compared to the $LiCoO_2$. In general, the appearance of the forbidden reflections indicates that the rhombohedral symmetry of the parent O3 phase is disturbed. Simulations illustrate that this can be achieved by placing a TM ion into the Li layer[24]. The formation of spinel phase after lithium extraction requires the displacement of some TM ions onto sites in Li layers. It should be noted that spinel phase was not observed in XRD pattern of delithiated material (Figure 1b) however; it was observed in electron diffraction data. This can be explained as follows. Electrons have much shorter wavelength compared to X-rays. This makes electron to scatter strongly because they interact with both the nucleus and the electrons providing detailed crystallographic information on each individual crystals that can be missed by X-ray which interacts only with the electrons.

In summary, both the observation of the broken rhombohedral symmetry and the appearance of spinel phase indicate that one or more TM species have moved out of the TM layer in agreement with conclusions drawn from the magnetic data. Since, Ni^{+2} has similar ionic radii as compared to the Li^+ ion, it can be speculated that the Ni^{+2} migrates to the lithium layer and occupies the vacant position generated during the process of lithium extraction process.

3.2. Delithiated material after ageing for 30 and for 45 days at 75°C

3.2.1 X-ray diffraction and magnetic behavior of delithiated and aged materials

The XRD spectra of the aged delithiated materials are shown in figure 1c (30 days) and d (45 days), ageing-*T*= 75°C. The corresponding lattice parameters are given in table 1. The inset in

figure 2 illustrates that the (003) peak shifts back towards higher angles with prolonged annealing time corresponding to a decrease in c lattice parameter with respect to the delithiated state. The distance between the peaks in (006)/ (102) and (108)/ (110) doublets increases, accompanied by a change in the c/a ratio. The decrease in c/a ratio indicates a rearrangement in the cation distribution as would be expected in case of the formation of spinel phase. This observation is supported by selected area electron diffraction studies (see below). Below we first present the magnetic responses and determine the oxidation states of the transition metal ions before the microstructural analysis which is given in the next section.

The temperature dependence of the magnetic susceptibility of the aged material is presented in figure 6. A comparison to the χ(T) curve of the delithiated material in figure 2 shows that both curves follow the same pathway. The material is paramagnetic at higher temperature (*T* > 100 ^{O}C) and shows an increase in magnetic susceptibility at lower temperature. The effective magnetic moments after aging were calculated as described in section 3.1.1 and the results are given in table 2. Comparison to the results obtained for the delithiated material shows that the effective magnetic moments remain approximately constant during ageing. Therefore, it is concluded that the oxidation states of the transition metal ions did not change during annealing (see table 2). In figure 4 it can be seen that the M(H) curves after ageing resembles that of the delithiated material except the slope of the curves are steeper in aged material. This indicates that the Ni^{+2}/Li^{+} interchange has been increased in all the aged material which could also be confirmed by their selected area electron diffraction data (see below). Over all, no significant change in magnetic responses before and after thermal aging of lithium deficient material was observed which suggests good thermal stability of this compound. For comparison, in a study on the thermal behavior of $Li_{1-x}CoO_2$ [22,29] we found that Co_3O_4 spinel formed after prolonged aging which could be identified from strong antiferromagnetic ordering at lower temperature. In this present work on aged $Li_{0.80}Ni_{1/3}Mn_{1/3}Co_{1/3}O_2$ no antiferromagnetic ordering is observed. This is

because the presence of Mn^{+4} ions lends thermal stability to the lattice of the $LiNi_{1/3}Mn_{1/3}Co_{1/3}O_2$ compound as reported in literature.[31]

3.2.2 *Microstructure of the delithiated and aged material*

The results of the diffraction analysis of powder particles of the material aged for 30 d and 45 d are presented in table 3. For both annealing times the amount of O3 phase has decreased from 60% after delithiation to 40% (8 of 20 particles) after heat treatment. At the same time the amount of spinel phase has increased to a maximum of 60% after 30 d of annealing, and to an amount of 45% after 45 d annealing time. After prolonged annealing for 45 d slightly fewer particles with spinel structure are observed than after 30 d as is also evident from relative intensities in the xrd spectra in Fig. 1. The difference is made up of spinel type particles that have additional forbidden {1-100} reflections (2 out of 20, see figure 8 b) or particles which show forbidden reflections (1 out of 20). This observation indicates that further structural modifications take place during prolonged anneal that are not understood yet. The intensity of the forbidden reflections is stronger compared to observations in the delithiated material which may indicate that more Ni^{+2} has moved to lithium layer increasing Li^{+}/Ni^{+2} disorder as compared to the delithiated material (see figure 8b) which is in agreement with the magnetic behavior explained above. Figure 8 represents a bright field TEM image and the corresponding SAED pattern of a particle with a spinel structure. The morphology of some of the aged particles shows defects parallel to (0001) planes that have been described as mille feuille morphology in an earlier report on cycled $LiNi_{1/3}Mn_{1/3}Co_{1/3}O_2$ [14,32] (see figure 7a highlighted in circle).

In summary, the change in microstructure during delithiation and ageing can be explained as follows and also represented in figure 9. In the starting material, all the ions occupy their respective crystallographic sites and no disorder (presence of Ni^{+2} ions in the lithium layer) is observed (figure 9 a). The delithiation process involves the extraction of lithium ions from

octahedral sites creating vacancies in the lithium layer. The lithium extraction also increases the interlayer repulsion and expansion of the unit cell occurs resulting in the increase in c-lattice parameter. Due to similar ionic radii of Ni^{+2} ions as compared to Li^{+} ions, this process is accompanied by the migration some of Ni^{+2} ions to the octahedral sites of the lithium layers to fill the vacancies (figure 10 b). After thermal ageing, a higher fraction of particles show cubic spinel structure and the observed forbidden reflections have a higher intensity which suggests that more Ni^{+2} ions have migrated to the lithium layer. At the same time, strong ferromagnetic hysteresis loop as would be expected from 180° interlayer Ni^{+2}-O-Mn^{+4} interaction, was not observed in the M/H curves from the aged materials. To understand this behavior, the Curie-Weiss temperature was calculated from the magnetic susceptibility curves, see table 2. The Curie-Weiss temperature becomes more negative in the aged material and is lowest for the material, which was aged for the longest duration. As discussed in the introduction, the presence of Ni^{+2} in the lithium layer may create the ferromagnetic and/or antiferromagnetic exchange depending on the ions that participate in the exchange interaction. The more negative values of the Curie-Weiss temperature in the aged material suggests that the 180° interlayer Ni^{+2}-O-Ni^{+2}intercation, which is strongly antiferromagnetic in nature, dominates over the 180° interlayer Ni^{+2}-O-Mn^{+4} interaction which is ferromagnetic. Therefore, during ageing a significant amount of Ni^{+2} has migrated to the vacancies in the lithium layer and increases the Ni^{+2}/Li^{+} disorder in the aged materials (figure 9 c). It is believed that due to presence of Ni^{+2}/Li^{+} disorder, decrease in the capacity can be observed during lithium extraction from $LiNi_{1/3}Mn_{1/3}Co_{1/3}O_2$ cathode and substantial capacity fade can be expected during ageing process.

4. Conclusion

The microstructure and magnetic properties of $LiNi_{1/3}Mn_{1/3}Co_{1/3}O_2$ and its delithiated material were investigated before and after ageing. Selected area electron diffraction studies revealed that

the starting material has maximum percentage of O3 phase of which a small percentage is converted to spinel phase after lithium de-intercalation. During ageing of the delithiated material the microstructure changes prominently. The appearance of strong forbidden reflection {1-100} along [0001] direction in long termed aged material as well as formation spinel phase indicate prominent Ni^{+2}/Li^{+} disorder in the crystals. The oxidation states of the transition metals derived from the magnetic measurement for delithiated material before ageing are similar to the materials after ageing which clearly suggests that there is no secondary phase like Co_3O_4 and/or $LiCo_2O_4$ present in the aged material. However, the change in particle morphology and significant microstructural changes observed in the aged materials surely indicates the thermal degradation pathways of this highly efficient cathode may occur via interlayer cation rearrangement.

Acknowledgement: This work was supported through the Louisiana Board of Regents, Grant No. LEQSF(2007012)-ENH-PKSFI-PRS-04 and LEQSF(200407)-RD-A36.

References:

(1) M. Wakihara; Yamamoto, O. *Lithium Ion Batteries - Fundamentals and Performance*; Wiley-VCH, 1998.

(2) D. Linden; Reddy, T. B. *Handbook of Batteries.*; 3rd ed.; MacGraw Hill Handbooks, 2002.

(3) J.R. Dahn; E. W.Fuller; M. Obrovac; Sacken, U. V. *Solid State Ionics* **1994**, *69*, 265-270.

(4) T. Ohzuku; Y. Makimura *Chemistry Letters* **2001**, *7*, 6423.

(5) I. Belharouak; Y.K. Sun; J. Liu; K. Amine *Journal of Power Sources* **2003**, *123*, 247.

(6) J.W. Wen; H.J. Liu; H. Wu; C.H. Chen *Journal of Materials Science* **2007**, *42*, 7696.

(7) N. Yabuuchi; Y. Koyama; N. Nakayama; T. Ohzuku *Journal of The Electrochemica Society* **2005**, *152*, A1434.

(8) M.S. Whittingham *Chemical Review* **2004**, *104*, 4271.

(9) R. D. Shannon *Acta Crystallographica A.* **1976**, *32*, 756.

(10) G Dutta; A Manthiraman; Goodenough, G. B. *Journal of Solid State Chemistry* **1992**, *96*, 123.

(11) T. Nedoseykina; S.-S. Kim; Y. Nitta *Electrochemica Acta* **2006**, *52*, 1467.

(12) K.-S. Lee; S.-T.Myung; J. Prakash; H.Yashiro; Y.-K.Sun *Electrochemica Acta* **2008**, *53*, 3065.

(13) Y.S. Meng; G. Ceder; C.P. Grey; W.-S. Yoon; M. Jiang; J. Breger; Y.Shao-Horn *Chemistry of Materials* **2005**, *17*, 2386.

(14) H. Gabrisch; R. Yazami *Electrochemical and Solid-State Letter* **2010**, *13*, A88.

(15) M.Ma; Natasha A. Chernova; Brian H. Toby; Peter Y. Zavalij; Whittingham, M. S. *Journal of Power Sources* **2007**, *165*, 517.

(16) Natasha A. Chernova; M.Ma; J. Xiao; M.S. Whittingham; J. Breger; Grey, C. P. *Chemistry of Materials* **2007**, *19*, 4682.

(17) D Mohanty; P. Paudel; H. Gabrisch *Solid State Ionics* **2010**, *181*, 914.

(18) Natasha A. Chernova; Gene M. Nolis; Fredrick O. Omenya; H. Zhou; and, Z. L.; Whittingham, M. S. *Journal of Materials Chemistry* **2011**, *21*,9865.

(19) Hertz, J. T.; Huang, Q.; McQueen, T.; Klimczuk, T.; Bos, J. W. G.; Viciu, L.; Cava, R. J. *Physical Review B* **2008**, *77*, 075119

(20) Mukai, K.; Sugiyama, J.; Ikedo, Y.; Andreica, D.; Amato, A.; Brewer, J. H.; Ansaldo, E. J.; Russo, P. L.; Chow, K. H.; Ariyoshi, K.; Ohzuku, T. *Journal of Physics and Chemistry of Solids* **2008**, *69*, 1479.

(21) Sugiyama, J.; Nozaki, H.; Brewer, J. H.; Ansaldo, E. J.; Morris, G. D.; Delmas,

C. *Physical Review B* **2005**, *72*, 144424.

(22) D Mohanty; H. Gabrisch *Solid State Ionics* **2011**, *194*, 41.

(23) X. Zhang; A. Mauger; F.Gendron; L.Qi; H.Groult; Perriguad, L.; C.M.Julien *Electrochemical Society Transactions* **2009**, *16*, 11.

(24) H. Gabrisch; T. Yi; R. Yazami *Electrochemical and Solid-State Letter* **2008**, *11*, A119.

(25) X. Luo; X. Wang; L. Liao; X. Wang; S. Gamboa; P.J. Sebastian *Journal of Power Sources* **2006**, *161*, 601.

(26) H. Gabrisch; R. Yazami; Fultz, B. *Journal of Electrochemical Society* **2004**, *151*, A891.

(27) J.R. Dhan; U.von Sacken; Michal, C. A. *Solid State Ionics* **1990**, *44*, 87.

(28) X. Zhang; W. J. Jiang; A. M. Qilu; F. Gendron; C.M.Julien *Journal of Power Sources* **2010**, *195*, 1292.

(29) D. Mohanty; H. Gabrisch *Electrochemical Society Transactions* **2009**, *19*, 25.

(30) J.B. Goodenough *Physical Review* **1960**, *117*, 1442.

(31) W. Lu; I. Belharouak; D.R. Vissers; Amine, K. *Journal of Electrochemical Society* **2004**, *151*, A246.

(32) H. Gabrisch; D. Mohanty *Electrochemical Society Transactions* **2009**, *16*, 1.

(33) K. Momma, F. Izumi, *Journal of Applied Crystallography* **2008**, *41*, 653.

List of tables:

Figure captions:

Figure 5. (a) Bright field TEM image showing the corroding edge and (b) the corresponding selected area electron diffraction of $Li_{0.80}Ni_{1/3}Mn_{1/3}Co_{1/3}O_2$ which shows the faint {1-100} reflection

Figure 6. Variation of magnetic susceptibility vs. temperature of $Li_{0.80}Ni_{1/3}Mn_{1/3}Co_{1/3}O_2$ after ageing at $75^{O}C$ at 30 days and 45 days

Figure 7. (a) Bright filed TEM image showing mille feuille morphology and (b) corresponding selected area diffraction of $Li_{0.80}Ni_{1/3}Mn_{1/3}Co_{1/3}O_2$ after heat treatment for 75C 30days shows the spinel and O3 reflections

Figure 8.(a) Bright filed TEM image and (b) selected area electron diffraction of $Li_{0.80}Ni_{1/3}Mn_{1/3}Co_{1/3}O_2$ after heat treatment for 75C45days shows forbidden {1-100} reflection marked as triangle, spinel reflection marked as circle and O3 reflections marked as square

Figure 9: Representation of change in microstructure during the delithiation and ageing of $LiNi_{1/3}Mn_{1/3}Co_{1/3}O_{2.}$ In the starting material Li and Ni ions occupy their respective crystallographic site (a). Delithiation process involves the extraction of lithium from the lithium layer creating vacancies (blue empty circles) in the lithium layer as well as migration of Ni^{+2} to lithium layer (filled red circle) (b). Upon ageing the Ni^{+2}/Li^{+} disorder has been increased (c). See the text in detail. The crystal model was drawn by using VESTA[32]

Figures

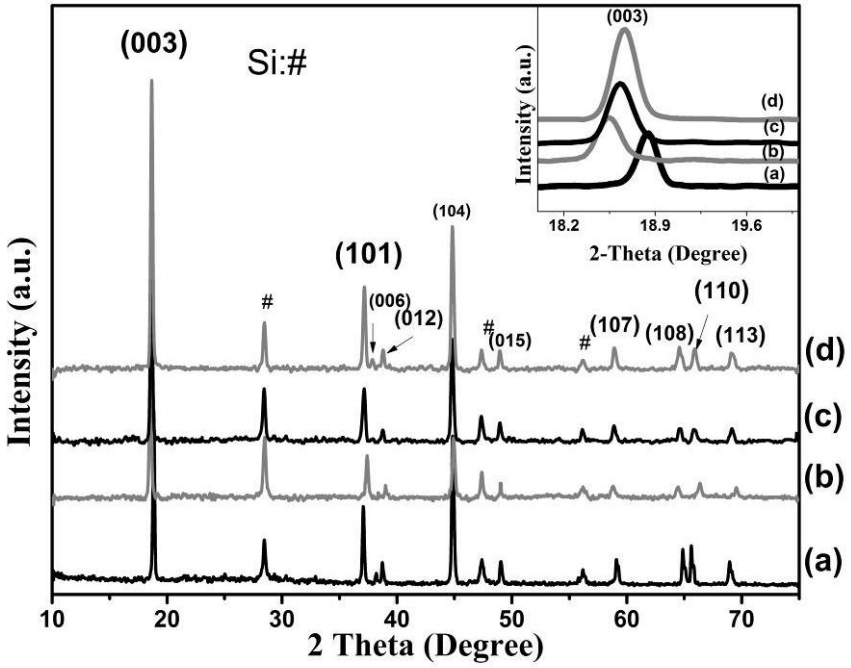

Figure 1. XRD of $LiNi_{1/3}Mn_{1/3}Co_{1/3}O_2$ (a) starting material, (b) delithiated material, (c) delithiated and aged at 75^{O}C for 30 days and (d) delithiated and aged at 75 ^{O}C for 45days.

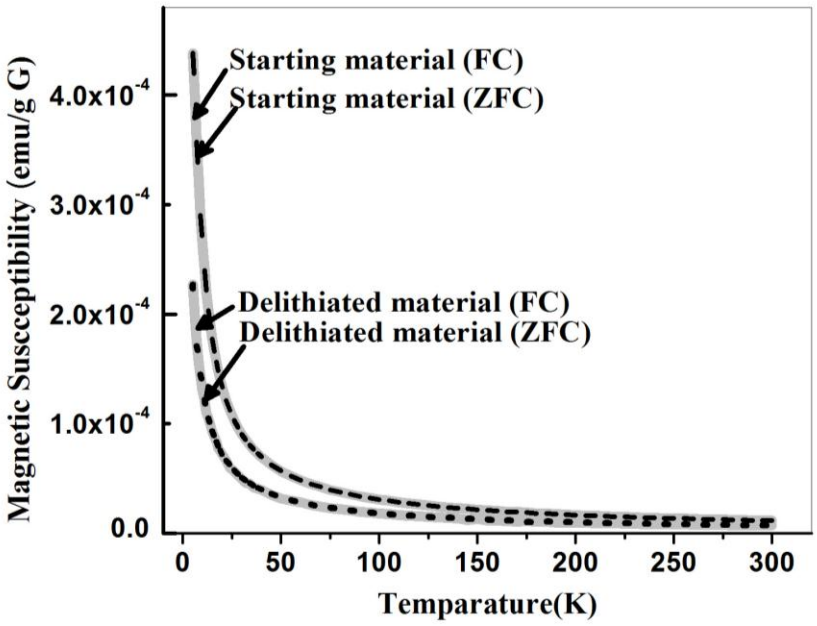

Figure 2. Variation of magnetic susceptibility vs. temperature of $LiNi_{1/3}Mn_{1/3}Co_{1/3}O_2$ and delithiated material $Li_{0.80}Ni_{1/3}Mn_{1/3}Co_{1/3}O_{2)}$ under field cooling (FC) and zero field cooling (ZFC) conditions.

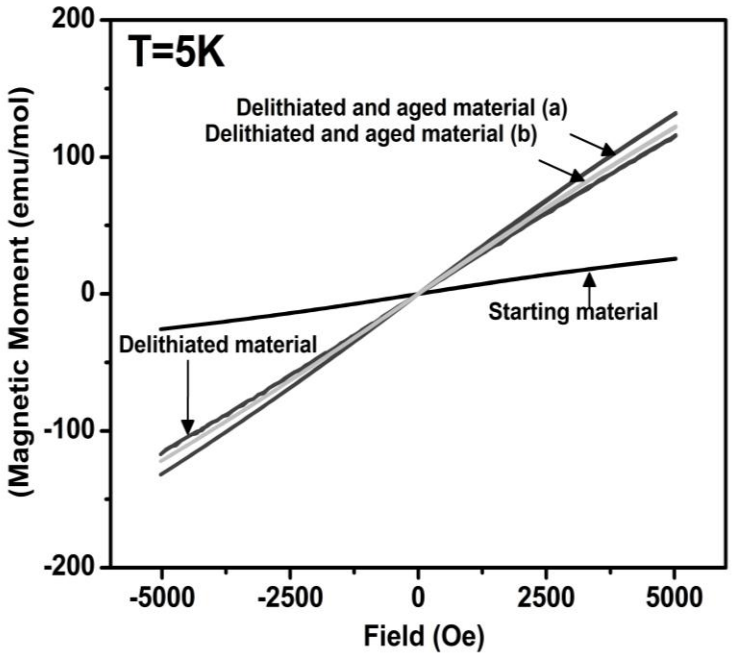

Figure 3. Magnetic moment (M) and magnetic field (H) of $LiNi_{1/3}Mn_{1/3}Co_{1/3}O_2$ starting material, delithiated material and delithiated material after ageing at 75^{O}C for 30 days (a) and 45 days (b)

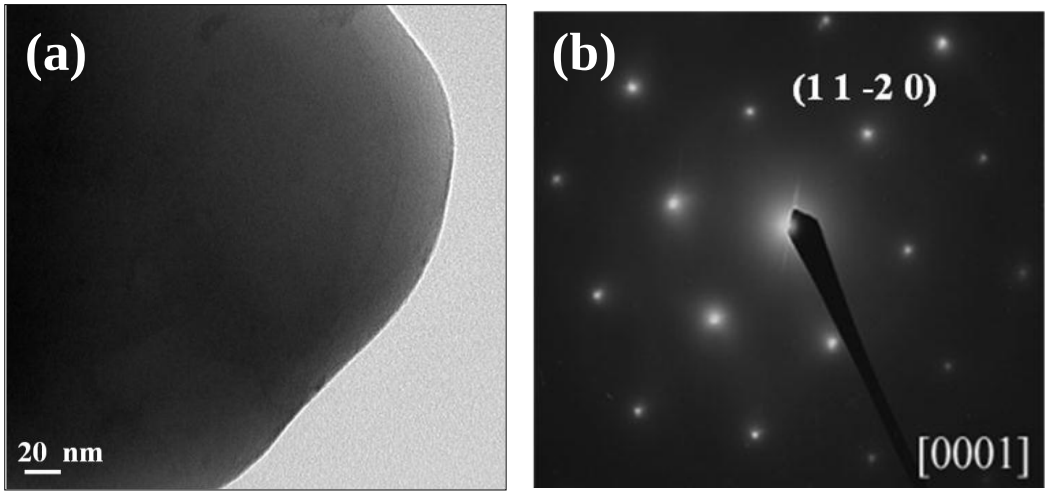

Figure 4. Example of (a) bright field TEM image and (b) the corresponding selected area diffraction of $LiNi_{1/3}Mn_{1/3}Co_{1/3}O_2$ starting material taken along [0001] zone axis shows O3 reflection without any in-plane ordering.

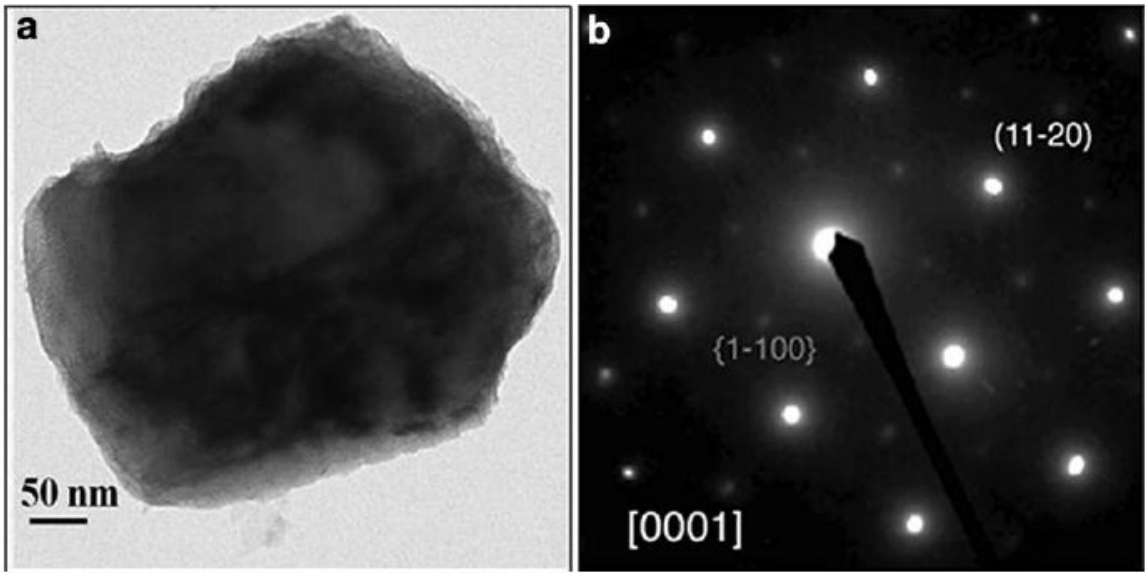

Figure 5. (a) Bright field TEM image showing the corroding edge and (b) the corresponding selected area electron diffraction of $Li_{0.80}Ni_{1/3}Mn_{1/3}Co_{1/3}O_2$ which shows the faint {1-100} reflection.

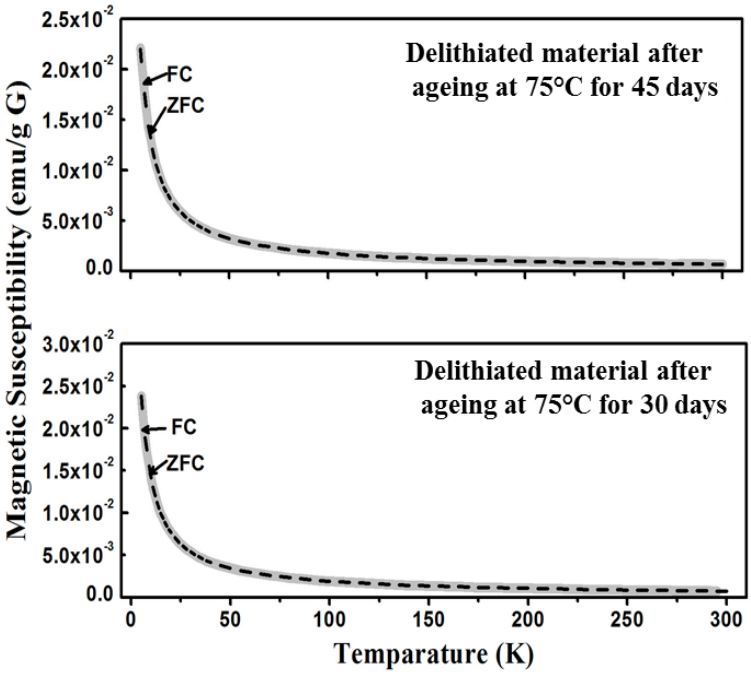

Figure 6. Variation of magnetic susceptibility vs. temperature of $Li_{0.80}Ni_{1/3}Mn_{1/3}Co_{1/3}O_2$ after ageing at 75^{O}C at 30 days and 45 days.

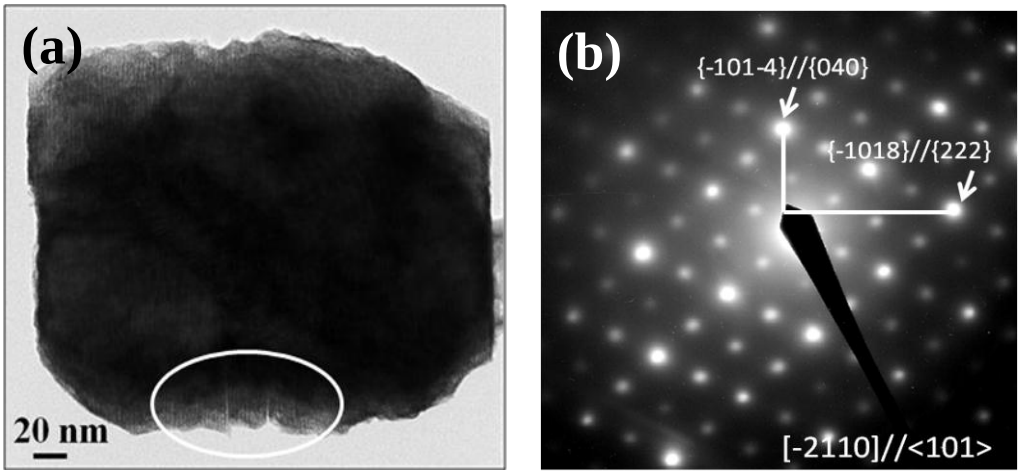

Figure 7. (a) Bright filed TEM image showing mille feuille morphology and (b) corresponding selected area diffraction of $Li_{0.80}Ni_{1/3}Mn_{1/3}Co_{1/3}O_2$ after heat treatment for 75C 30days shows the spinel and O3 reflections

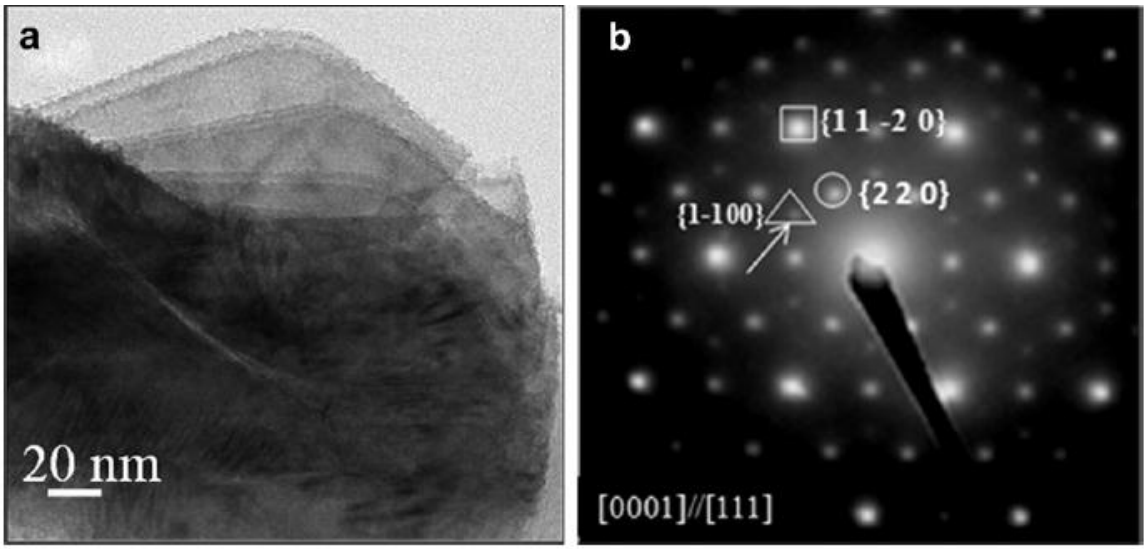

Figure 8.(a) Bright filed TEM image and (b) selected area electron diffraction of $Li_{0.80}Ni_{1/3}Mn_{1/3}Co_{1/3}O_2$ after heat treatment for 75C45days shows forbidden {1-100} reflection marked as triangle, spinel reflection marked as circle and O3 reflections marked as square .

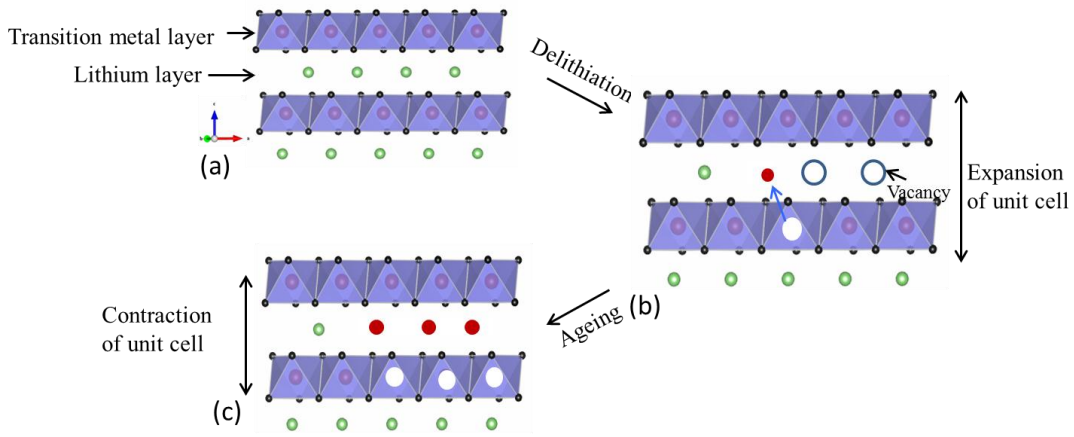

Figure 9: Representation of change in microstructure during the delithiation and ageing of $LiNi_{1/3}Mn_{1/3}Co_{1/3}O_{2.}$ In the starting material Li and Ni ions occupy their respective crystallographic site (a). Delithiation process involves the extraction of lithium from the lithium layer creating vacancies (blue empty circles) in the lithium layer as well as migration of Ni^{+2} to lithium layer (filled red circle) (b). Upon ageing the Ni^{+2}/Li^{+} disorder has been increased (c). See the text in detail. The crystal model was drawn by using VESTA[33].

Tables

Table 1: lattice parameters, and c/a ratio of $LiNi_{1/3}Mn_{1/3}Co_{1/3}O_2$ and its delithiated product before and after ageing at 75 ^{O}C for 30d and 45d

Materials	Lattice parameter [Å]
Starting material	c= 14.135 (2) a= 2.844 (2)
Delithiated material	c= 14.384(2) a= 2.822(2)
Delithiated material after ageing at 75^{O}C 30d	c= 14.289(2) a= 2.824(2)
Delithiated material after ageing at 75^{O}C 45d	c= 14.254 (2) a= 2.82(2)

Table 2: Composition, effective magnetic moments (calculated and experimental), corresponding oxidation states of transition metal ions, and the Curie-Weiss temperature of $LiNi_{1/3}Mn_{1/3}Co_{1/3}O_2$ and its delithiated material before and after ageing at 75 ^{O}C for 30d and 45d

Materials	ICP Composition	Experimental effective magnetic moment (μ_B)	Calculated effective magnetic moment (μ_B)	Oxidation states of transition metal ions	Curie- Weiss Temperature (K)
Starting material	$Li_{1\pm02}Co_{0.33\pm02}Mn_{0.33\pm02}Ni_{0.33\pm02}O_2$	2.69 ± 0.01	2.77	$Co_{0.33}^{+3}$(HS) $Mn_{0.33}^{+4}$(HS) $Ni_{0.33}^{+2}$(HS)	-59
Delithiated material	$Li_{0.80\pm02}Co_{0.33\pm02}Mn_{0.34\pm02}Ni_{0.34\pm02}O_2$	2.33 ± 0.1	1.76	$Co_{0.33}^{+3}$(LS) $Mn_{0.34}^{+4}$(HS/LS) $Ni_{0.23}^{+2}$(HS/LS) $Ni_{0.10}^{+4}$(LS)	-98
Delithiated material after ageing at 75^{O}C 30d	$Li_{0.80\pm02}Co_{0.31\pm02}Mn_{0.32\pm02}Ni_{0.34\pm02}O_2$	2.38 ± 0.01	1.78	$Co_{0.31}^{+3}$(LS) $Mn_{0.32}^{+4}$(HS/LS) $Ni_{0.24}^{+2}$(HS/LS) $Ni_{0.10}^{+4}$(LS)	-107
Delithiated material after ageing at 75^{O}C 45d	$Li_{0.80\pm02}Co_{0.30\pm02}Mn_{0.34\pm02}Ni_{0.32\pm02}O_2$	2.35 ± 0.05	1.75	$Co_{0.30}^{+3}$(LS) $Mn_{0.34}^{+4}$(HS/LS) $Ni_{0.22}^{+2}$(HS/LS) $Ni_{0.10}^{+4}$(LS)	-131

Table 3: Classification of diffraction patterns obtained from $LiNi_{1/3}Mn_{1/3}Co_{1/3}O_2$ and its delithiated products before and after ageing at 75 ^{O}C for 30d and 45d

Materials	**Starting material**	**Delithiated material**	**Delithiated material after ageing at 75^{O}C 30d**	**Delithiated material after ageing at 75^{O}C 45d**
O3	20/22 (90%)	12/20 (60%)	8/20 (40%)	8/20 (40%)
Spinel	2/20 (10%)	4/20 (20 %)	12/20 (60%)	9/20 (45%)
O3+forbidden	0	4/20 (faint) (20%)		1/20 (5%)
O3+forbidden+Spinel	0	0		2/20 (10%)
In-plane ordering	0	0		0
Total no. particles	22	20	20	20